Electronic Supplementary Material (ESI) for Sustainable Energy & Fuels.

Supplementary information (SI)

For

Homogeneous visible light-driven hydrogen evolution using the molecular molybdenum sulfide model $[Mo_2S_{12}]^{2-}$

Ashwene Rajagopal, Felix Venter, Timo Jacob, Lydia Petermann, Sven Rau, Stefanie Tschierlei, and Carsten Streb*
Ulm University, Albert-Einstein-Allee 11, 89081 Ulm, Germany

Table of Contents

1. Instrumentation

UV-Vis spectroscopy: UV-Vis spectroscopy was performed on a Shimadzu UV-2450 spectrophotometer, Varian Cary 50 spectrophotometer or Varian Cary 5G spectrophotometer. All systems were used with standard cuvettes (d = 10.0 mm).

Emission spectroscopy: Emission spectroscopy was performed on a Jasco FP-8500 spectrofluorometer. Standard emission cuvettes (d = 10.0 mm, V = 3 ml) were used.

Single-crystal X-Ray Diffraction (XRD): single-crystal XRD data were collected on an Agilent SuperNova CCD single-crystal X-ray diffractometer (λ (Mo Kα) = 0.71073 Å) equipped with a graphite monochromator.

Dynamic light scattering (DLS): DLS measurements were performed on a Malvern Instruments Zetasizer ZEN 3600 with a particle size detection limit of 0.6 nm – 6000 nm and a particle concentration detection limit of 0.001 – 1 mass-% (for particles in the 100-1000 nm size range).

Inductively coupled plasma atomic emission spectrometry (ICP-AES) was performed on a Perkin Elmer Plasma 400 spectrometer.

Gas chromatography: Gas-chromatography was performed on a Bruker Scion GC/MS, with a thermal conductivity detector 15 (column: molecular sieve 5A 75 m × 0.53 mm, oven temperature 70 °C, flow rate 25 ml min^{-1}, detector temperature 200 °C) with Argon as a carrier gas. The GC was calibrated by direct injection of known amounts of H_2 gas.

Scanning electron microscopy / energy dispersive X-ray spectroscopy (SEM-EDX): SEM was performed on a Zeiss DSM 962 electron microscope in combination with an EDAX EDS unit for energy dispersive X-Ray spectroscopy. The samples were mounted on carbon tabs and sputtered with carbon before the measurement. SEM studies were performed at an acceleration voltage of 5 kV. EDX measurements were performed at an acceleration voltage of 10 kV.

FT-IR spectroscopy: FT-IR spectroscopy was performed on a Shimadzu IR Prestige-21 FTIR spectrophotometer with a Golden Gate ATR unit. Signals are given as wavenumbers in cm^{-1} using the following abbreviations: vs = very strong, s = strong, m = medium, w = weak and b = broad.

Raman spectroscopy: Non-resonant Raman spectra of the samples excited at 785 nm were recorded with a micro-Raman setup (LabRam inverse, Jobin–Yvon–Horiba). This setup is equipped with an Olympus BX40 microscope and a video camera. The scattered light was detected by an air-cooled Symphony CCD camera operating at 298 K. An Olympus MPlan 10×0.25 objective focused the laser light on the samples. The grating of the spectrometer had 1800 lines/mm, and the validation of the wavenumber axis was done by using the Raman signals of TiO_2 (anatase). For excitation, a high power diode laser (SDL-XC30) with a wavelength of 785 nm was used.

Elemental analysis: Elemental analysis was performed on a Euro Vector Euro EA 3000 Elemental Analyzer.

General remarks: All chemicals were purchased from Sigma Aldrich, ABCR or ACROS and were of reagent grade. The chemicals were used without further purification unless stated otherwise.

2.1 Synthesis of {Mo_2}: $(NH_4)_2[Mo_2S_{12}].2H_2O$ was prepared by a modification of synthesis reported by Wu *et al.*[1] $(NH_4)_6[Mo_7O_{24}]$ x $4H_2O$ (2 g, 1.62 mmol) was dissolved in 20ml of deionized water. 1.5 g of NH_2OHxHCl dissolved in 15ml of water and was added dropwise to the solution of $(NH_4)_6[Mo_7O_{24}]$ x $4H_2O$. 30ml of $(NH_4)_2S_x$ solution (> 25 wt.-%) was added, and the solution was heated to 50°C for one hour, cooled to room temperature and filtered. The filtrate was heated to 90°C for 5 hours, cooled to room temperature and filtered into a Schlenk flask. To this filtrate 10ml of $(NH_4)_2S_x$ (> 25 wt.-%) was added, and the solution was stirred under argon overnight. A black precipitate was obtained, isolated by filtration and washed with ice-cold water and 50 ml isopropanol. To remove the excess sulfur, the crude product was washed with 30 ml of CS_2 and 20ml of diethyl ether. The compound $(NH_4)_2Mo_2S_{12}$ x $2H_2O$ was vacuum dried and stored under argon.

Elemental analysis for $(NH_4)_2[Mo_2S_{12}]$ x $2H_2O$ in wt.-% (calcd.): Mo 29.85 (30.05), S 59.16 (58.88) H 1.85 (1.86), N 4.50 (4.30).

3. Characterization

3.1 Powder X-ray diffraction: powder XRD shows a match for the published $(NH_4)_2Mo_2S_{12}$ x $2H_2O$ diffractogram.

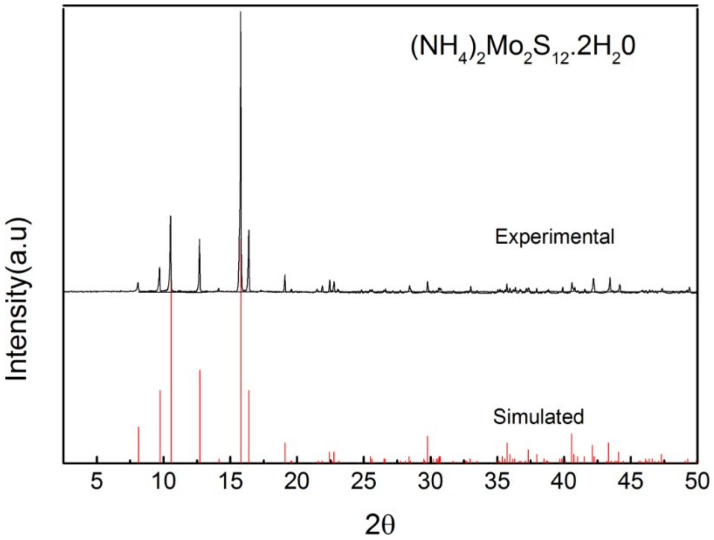

Figure S1: Powder x-ray diffraction pattern of $(NH_4)_2[Mo_2S_{12}]$ x $2H_2O$ (experimental (black curve) and simulated (red curve)).

3.2 Infrared spectroscopy: The signals at 522 cm^{-1} and 541 cm^{-1} are associated with the S-S stretching mode (terminal and bridging disulfide, respectively). The broad band at 960 cm^{-1} is associated with Mo-S stretching modes. The signal at 1400 cm^{-1} is related to NH_4^+ .

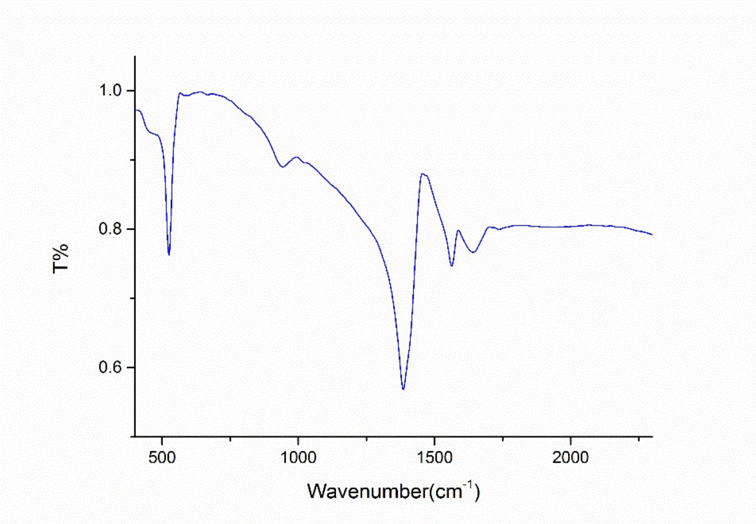

Figure S2: Infrared spectroscopy of $(NH_4)_2[Mo_2S_{12}].2H_2O$

3.3 Thermogravimetric analysis: TGA analysis agrees with the thermal decomposition of $(NH_4)_2[Mo_2S_{12}]$ x $2H_2O$. Both water molecules are lost at T ~ 60 °C. Between 100˚C to 200˚C, cluster degradation, possibly due to loss of sulfur is observed.

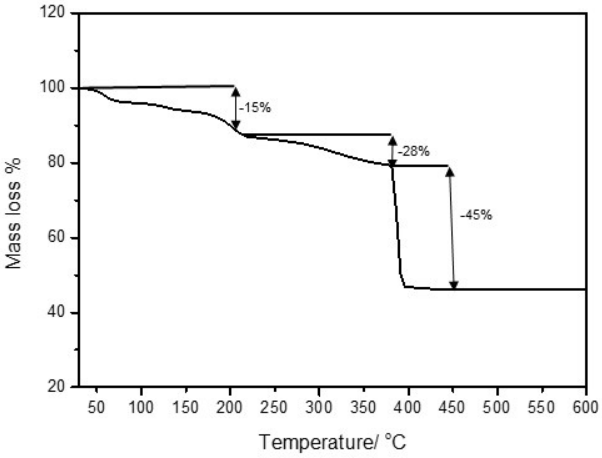

Figure S3: Thermogravimetric analysis for $(NH_4)_2[Mo_2S_{12}]$ x $2H_2O$.

4. Catalytic section

4.1. Light-driven hydrogen evolution studies:

Solvents: All solvents were purged with high-purity argon before each measurement to remove traces of oxygen.

Standard reaction setup: 5 mL GC vials were filled with 2 mL of the reaction mixture under inert conditions (containing solvent, the respective catalyst, photosensitizer ($[Ru(bpy)_3]PF_6$) and electron donor (ascorbic acid) at the concentrations specified. The catalyst is soluble in dimethyl formamide (DMF).So initially 0.5 mM concentrated solution of the catalyst was prepared in DMF and then further diluted twice in degassed methanol solution. *Standard conditions:* solvent: MeOH:H_2O, 10:1, v:v; [catalyst] = 5 x 10^{-7} M, $[Ru(bpy)_3]^{2+}$ = 2 x 10^{-5} M, [ascorbic acid] = 0.01 M). The vials were sealed with a septum cap. The samples were irradiated with a LED light source (λ_{max} = 470 nm) in a custom-built, air-cooled photoreactor. Hydrogen evolution was quantified by gas-chromatography. Each measurement was carried out in triplicate, the values reported are the resulting average. **Control experiments** were performed and showed no hydrogen evolution when the samples are not irradiated, or when catalyst**,** $[Ru(bpy)_3]^{2+}$ or ascorbic acid are absent.

Definitions: $TON = n(H_2) / n(\text{catalyst})$ $TOF = TON / t_{\text{irradiation.}}$

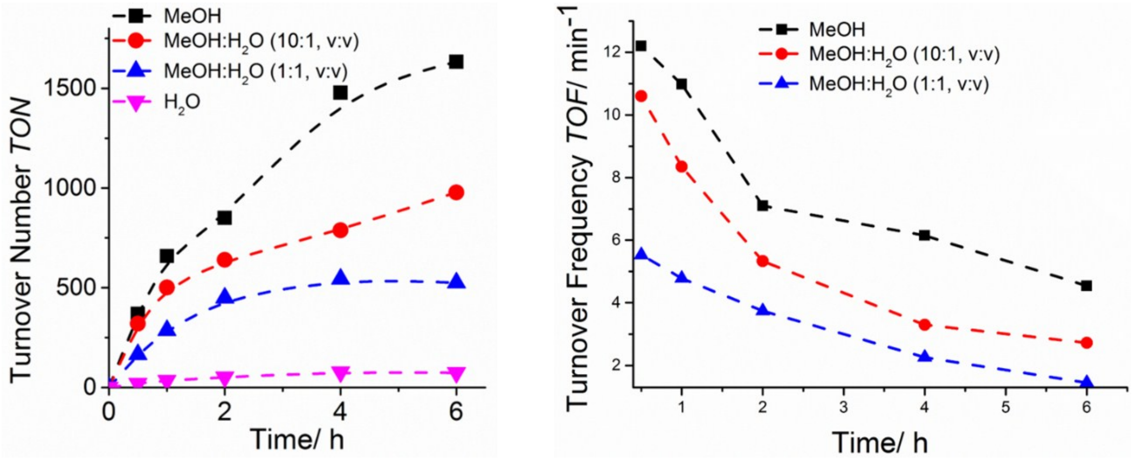

Figure S4a. Turnover Number (TON) and Turnover Frequency (TOF) for the HER catalysis of **{Mo_2}** in various MeOH:H_2O solvent mixtures.

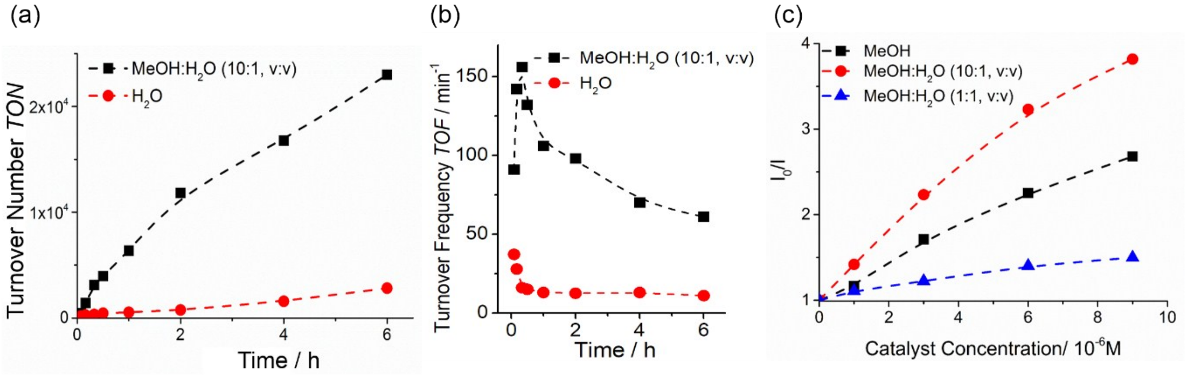

Figure S4b. (a) Turnover number (*TON*) for the HER catalysis of **{Mo_3}**. (b) Turnover frequency (TOF) for the HER activity of **{Mo_3}**. (c) Stern-Volmer-plot for the quenching of the photosensitizer $[Ru(bpy)_3]^{2+}$ by **{Mo_3}** in different solvents.

4.2. Catalyst concentration variation

Variation of the catalyst concentration showed that under the given experimental conditions, high reactivity is observed at concentrations in the range of 5 x 10^{-7} M. Higher catalyst concentrations led to colloid formation and precipitation, resulting in low *TON*s. Conditions: solvent: MeOH:H_2O, 10:1, v:v, $[Ru(bpy)_3]^{2+}$ = 2 x 10^{-5} M, [ascorbic acid] = 0.01 M.

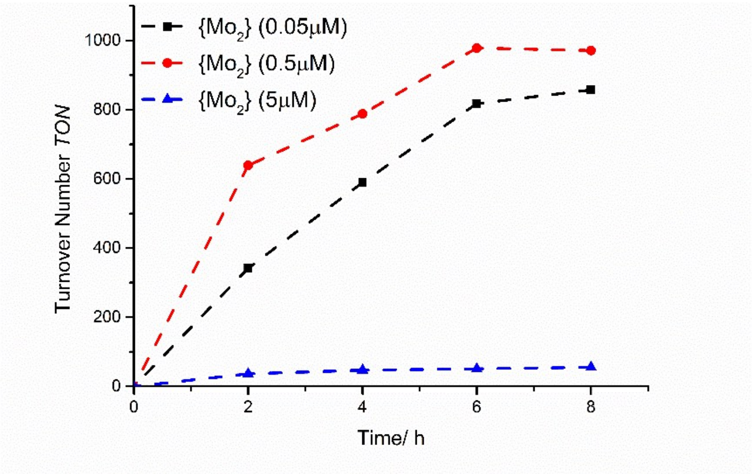

Figure S5. Turnover Number (TON) for the HER catalysis of **{Mo_2}** in MeOH:H_2O, 10:1, v:v under varying concentration of the catalyst

4.3. Ascorbic acid concentration variation

Catalytic experiments at varying ascorbic acid concentrations showed low HER activity at low ascorbic acid concentrations (0.001 M), while virtually identical reactivity is noted at ascorbic acid concentrations of 0.01 M and 0.1 M.

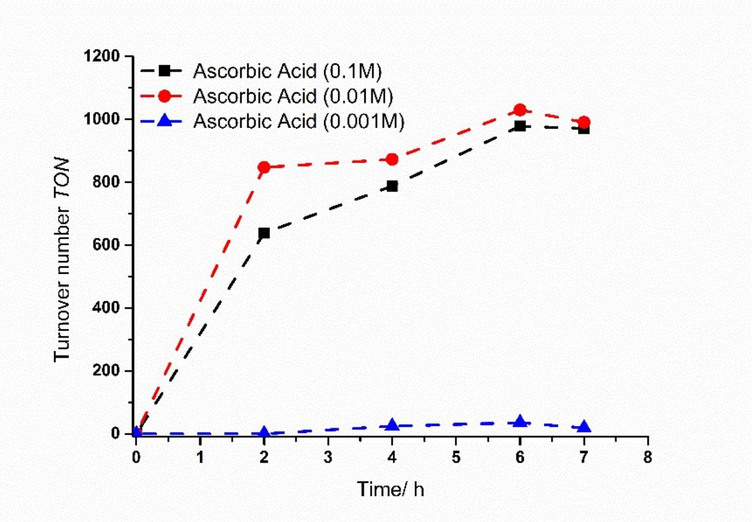

Figure S6. Turnover number for the HER activity of **{Mo$_2$}** in MeOH:H$_2$O, 10:1, v:v at varying ascorbic acid concentrations.

4.4. Influence of 2,2-bipyridine and chloride as competing coordinating ligand

In the presence of higher concentrations (2mM) of bpy (2,2- bipyridine) or chloride (nBu$_4$NCl), reduced HER reactivity is observed at reaction times $t_{\text{irradiation}}$ > 4 h, suggesting that ligand exchange occurs on the hour timescale as depicted in Figure 3a. The ligand exchange can be studied by using UV-Visible spectroscopy of **{Mo$_2$}** in the presence of coordinating ligands under irradiation conditions.

UV-Vis spectroscopy of the reaction solution indicates characteristic spectral changes after prolonged irradiation $t_{\text{irradiation}}$ > 3 h).

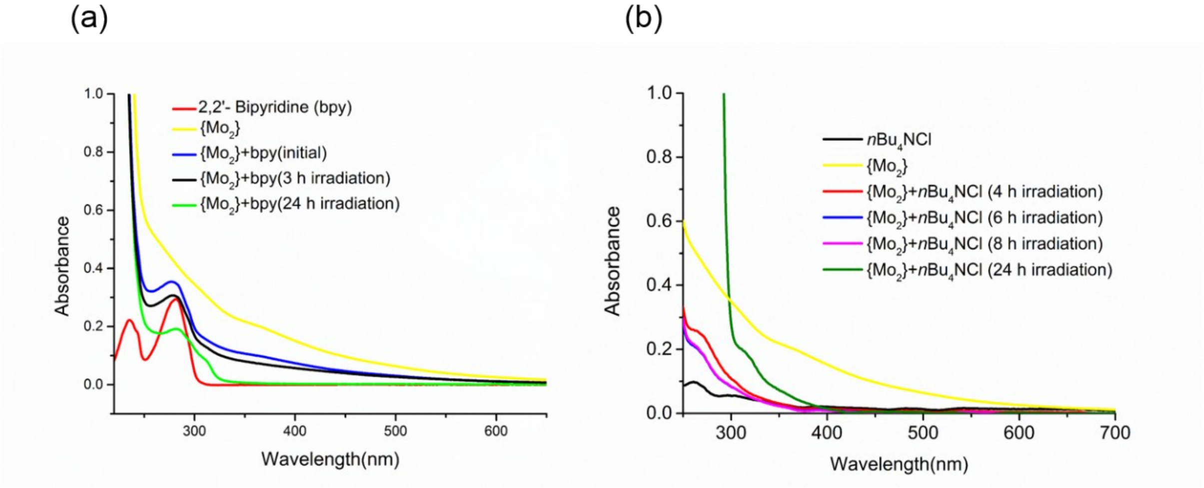

Figure S7. (a) and (b) UV-Visible spectroscopic analysis of a solution of **{Mo$_2$}** (0.2 mM) and 2,2´-bipyridine (2 mM), nBu$_4$NCl (2mM) under irradiation.

4.5. Effects of coordinating ligands on the catalytic activity of $\{Mo_2\}$ and $\{Mo_3\}$

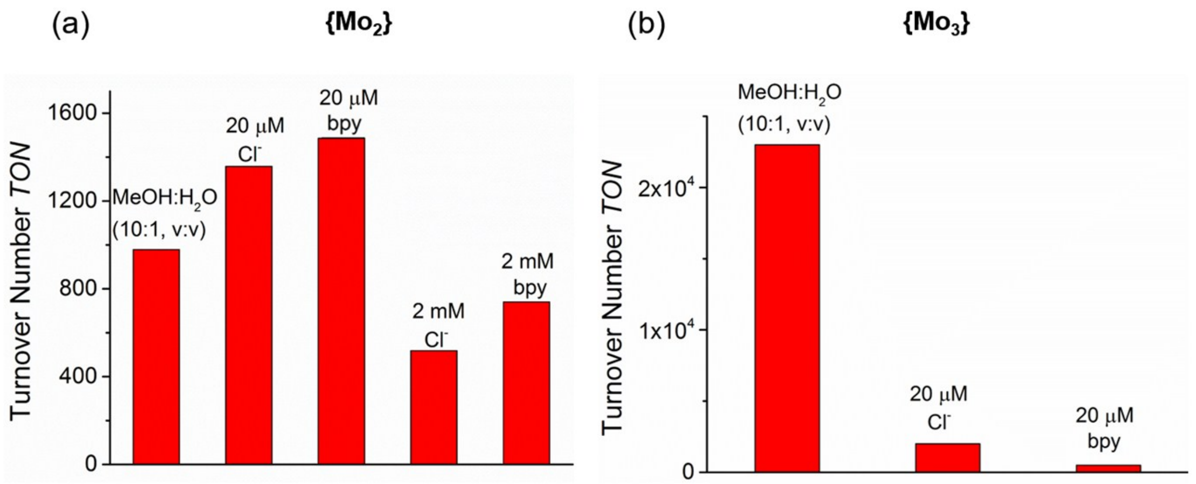

Figure S8. Bar diagrams of the HER activity of **$\{Mo_2\}$** (a) and **$\{Mo_3\}$** (b) in the presence of Cl^- and 2,2'- bipyridine (bpy) ligands. Catalytic conditions: $[\{Mo_2\}]$ = 0.5 μM, $[[Ru(bpy)_3]^{2+}]$ = 20 μM, solvent = $MeOH:H_2O$ (10:1, v:v). Catalytic conditions: $[\{Mo_3\}]$ = 0.3 μM, $[[Ru(bpy)_3]^{2+}]$ = 20 μM, solvent = $MeOH:H_2O$ (10:1, v:v). Note that the reason for the increased HER activity of **$\{Mo_2\}$** at 20 μM competing ligand concentrations is thus far unexplored.

4.6. Photosensitizer deactivation affecting the catalysis activity:

UV-Vis spectroscopy (see below) indicated that the photosensitizer $[Ru(bpy)_3]^{2+}$ is degraded after irradiation times > 5h. The degradation is assigned to a loss of bipyridine ligands based on previous literature.[2] In order to assess the remaining reactivity of $\{Mo_2\}$, we performed the standard catalytic reaction ($t_{irradiation}$ = 6 h) and then added a second aliquot of $[Ru(bpy)_3]^{2+}$ photosensitizer (under inert conditions). Continued hydrogen evolution was observed under irradiation, leading to maximum *TONs* of *ca*. 1750 after $t_{irradiation}$ = 12 h, see below.

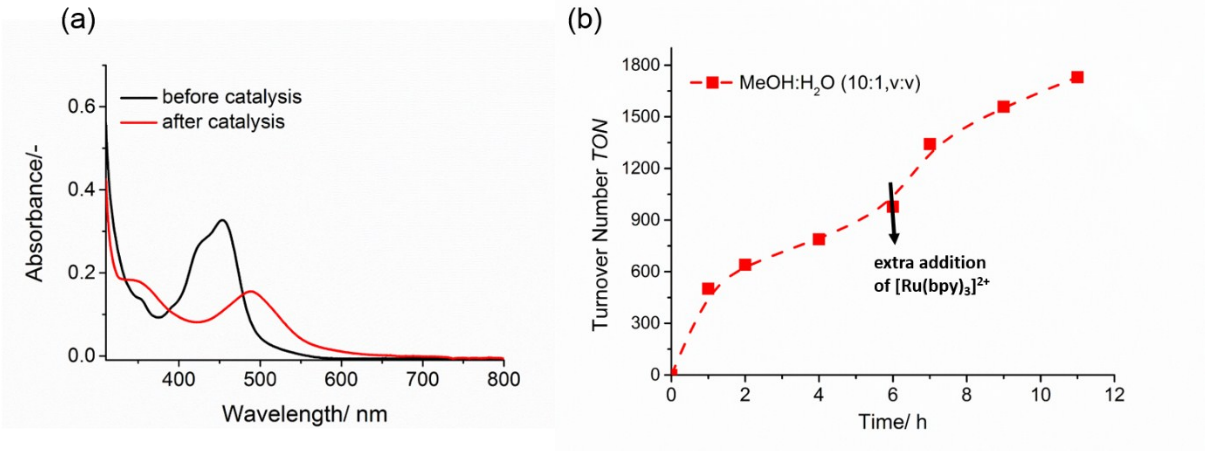

Figure S9. (a) UV-Visible spectra showing the degradation of the photosensitizer $[Ru(bpy)_3]^{2+}$ under catalytic conditions. Conditions: $MeOH:H_2O$ (10:1, v:v), **$[\{Mo_2\}]$** = 0.5 μM), $[[Ru(bpy)_3]^{2+}]$ = 20 μM, [ascorbic acid] = 0.01 M **(b)** Sustained HER activity upon addition of a second aliquot of photosensitizer after 6 h. Conditions: $MeOH:H_2O$ (10:1, v:v), $[\{Mo_2\}]$ = 0.5 μM), $[[Ru(bpy)_3]^{2+}]$: 1st aliquot: 20 μM; 2nd aliquot: 20 μM, [ascorbic acid] = 0.01 M.

5. Colloid detection procedure

To exclude the formation of colloidal particles (e.g. by precipitation of $[Ru(bpy)_3]^{2+}$/$[Mo_3S_{13}]^{2-}$ salts) in the above reaction system, a literature-known colloid detection procedure using dynamic light scattering (DLS), micro-filtration (using a 0.2 μm pore size PTFE syringe filter), UV-Vis spectrometry and scanning electron microscopy / energy-dispersive X-ray spectroscopy was performed.[3] For all samples reported, no colloid formation was observed over the course of the catalytic reaction.

5.1. Micro-filtration of the solutions using a 0.2 μm pore size PTFE syringe filter and UV-Vis spectroscopic analysis of the solutions before and after filtration show no significant change in the UV-Vis spectroscopic trace of the catalyst-containing solutions. **SEM-EDX analysis** of the filter membrane show no particles and do not feature EDX signals for Mo, S or Ru, see below.

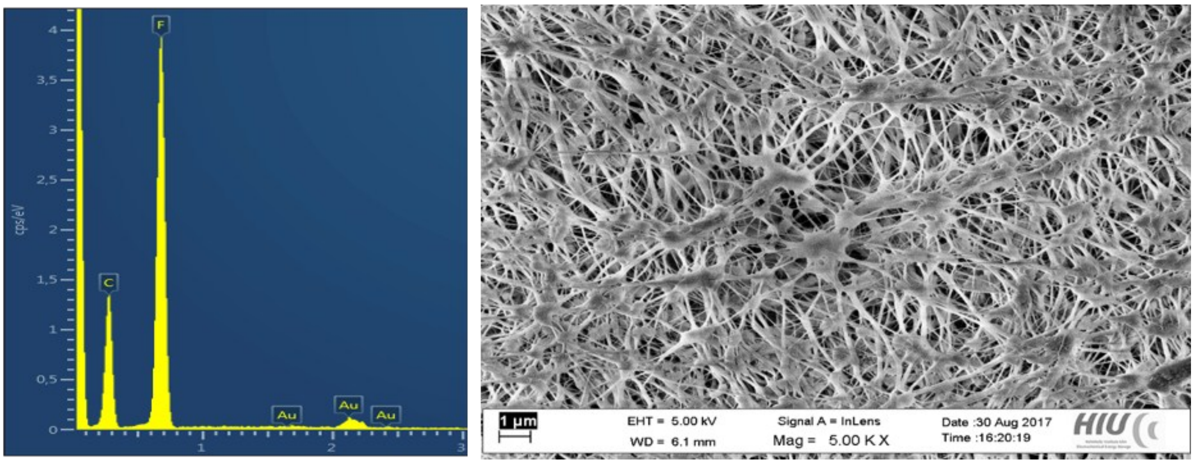

Figure S10. Left. EDX analysis of the filter membrane (fibrous structure) after filtration shows that no colloidal particles (no Mo, S, Ru detected by EDX) are retained on the membrane. **Right.** Scanning Electron Microscopic SEM picture of the filter membrane after filtration of the catalytic solution.

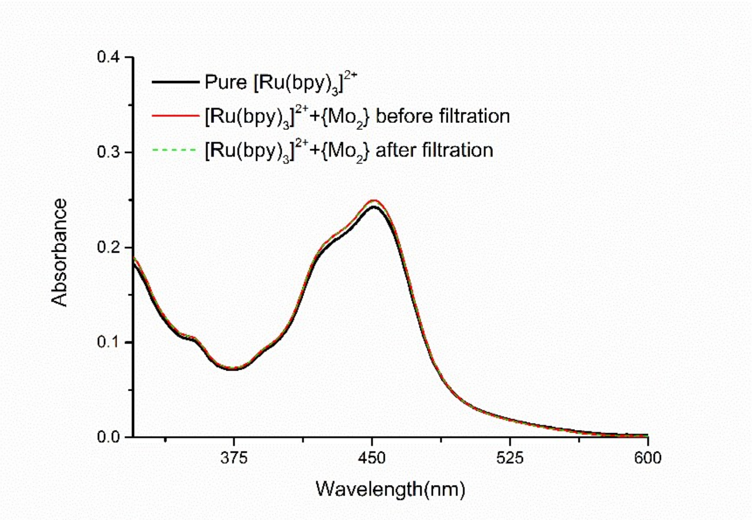

Figure S11. UV-Vis spectroscopic analysis of the reaction solution before and after micro-filtration. No changes are observed after filtration.

5.2. Dynamic Light Scattering: showed no particles in the reaction solution.

Dynamic light scattering for standard HER reaction solutions containing [**{Mo_2}**] = 5 × 10^{-7} M, [[Ru(bpy)$_3$]$^{2+}$] = 2 × 10^{-5} M, [ascorbic acid] = 0.01 M solvent, [*n*Bu_4Cl] = 2 x 10^{-5} M: MeOH:H_2O (10:1, v:v) before and after irradiation (λ_{max} =470 nm, $t_{irradiation}$ = 25 min) at room temperature.

Condition	**DLS average particle size / nm**	**DLS mean count rate / kcps**
Pure solvent	**-**	**25.56**
Reaction solution after irradiation	**-**	**90.41**
Reaction solution with TBACl before irradiation	**-**	**177.37**
Reaction solution with TBACl after irradiation	**-**	**101.47**

The DLS measurements showed a consistently negative measurement result for the specimens entered. This is to be fixed at the average count rate given in 1000 counts per second (kcps). The count rate indicates how many particle-scattered photons in the sample could be detected by the meter per second. It can be roughly assumed that kcps below 200 indicate that the sample does not contain any particles that scatter the incident light.

6. HER activity of {Mo_2} using a different photosensitizer

The HER activity of the catalyst was investigated in the presence of a different ruthenium based photosensitizer. Here, we used the literature-known species [Ru(tbbpy)$_2$(mmip)](PF_6)$_3$ (tbbpy = 4,4'-*tert*-butyl-2,2' bipyridine; mmip = 1,3-dimethyl-1*H*-imidazo[4,5-*f*][1,10] phenanthrolinium) which had been reported and photophysically studied before.[4,5] Stern-Volmer quenching studies showed significant interactions between this PS and **{Mo_2}** (see below).

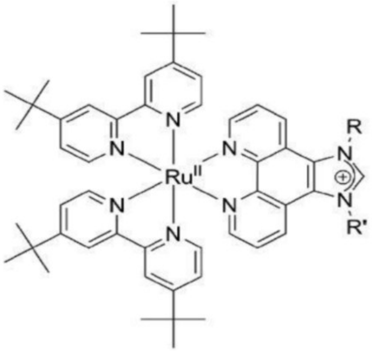

Figure S12. Structural representation of [Ru(tbbpy)$_2$(mmip)]$^{3+}$; R = R' = Me.

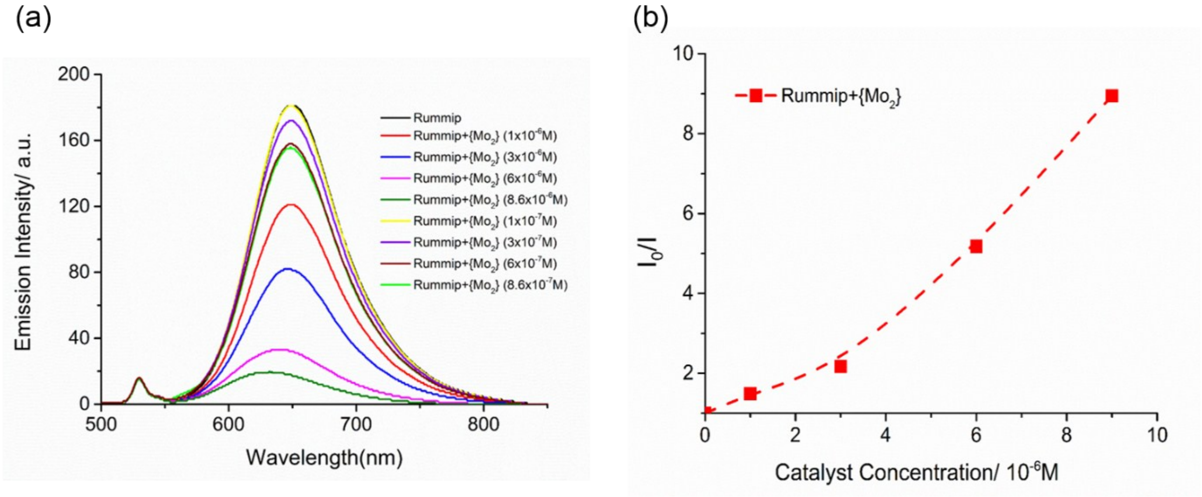

Figure S13. (a) Decrease of the emission intensity of the photosensitizer upon addition of the catalyst **{Mo_2}**. **(b)** Stern-Volmer plot of the quenching process. Conditions: solvent: $MeOH:H_2O$ 10:1, v:v; [catalyst] = 0 - 10 μM, $[[Ru(tbbpy)_2(mmip)]^{3+}]$ = 20 μM.

Light driven HER was performed using **{Mo_2}** as catalyst and $[Ru(tbbpy)_2(mmip)]^{3+}$ as photosensitizer under the standard conditions established before (10:1 $MeOH:H_2O$ as solvent, details see below). Compared with the initial tests with $[Ru(bpy)_3]^{2+}$, we observe slightly reduced activity based on TON, see below. Note however, that this system has not been optimized and was used under identical conditions to the original $[Ru(bpy)_3]^{2+}$ system.

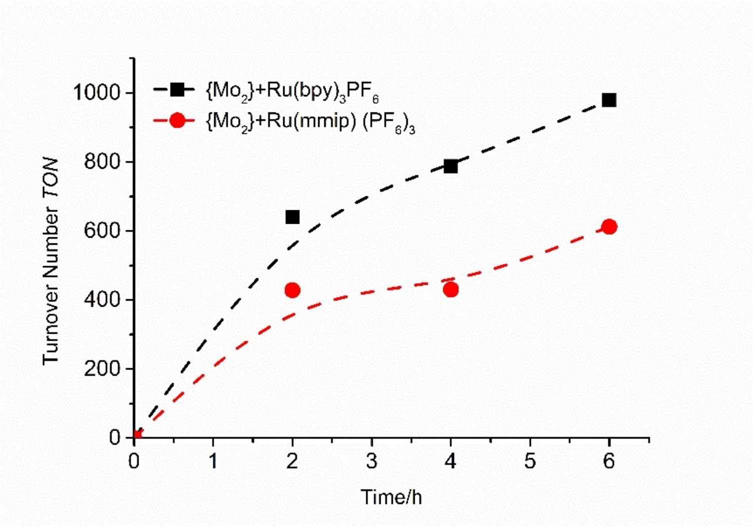

Figure S14. HER activity of **{Mo_2}** in the presence of the photosensitizer . Catalytic conditions: $MeOH:H_2O$ (10:1, v:v), [**{Mo_2}**] = 0.5 μM), $[[Ru(bpy)_3]^{2+}]$ = 20 μM, [Ru(mmip)] = 20 μM, [ascorbic acid] = 0.01 M and irradiation at 470 nm.

7. Literature References

1 Z. Huang, W. Luo, L. Ma, M. Yu, X. Ren, M. He, S. Polen, K. Click, B. Garrett, J. Lu, K. Amine, C. Hadad, W. Chen, A. Asthagiri and Y. Wu, *Angew. Chem. - Int. Ed.*, 2015, **54**, 15181–15185.

2 A. J. V.Balzani, *Coord. Chem. Rev.*, 1988, **84**, 85–277.

3 B. Kirchhoff, S. Rau and C. Streb, *Eur. J. Inorg. Chem.*, 2016, **2016**, 1425–1429.

4 R. Staehle, C. Reichardt, J. Popp, D. Sorsche, L. Petermann, K. Kastner, C. Streb, B. Dietzek and S. Rau, *Eur. J. Inorg. Chem.*, 2015, **2015**, 3932–3939.

5 L. Petermann, R. Staehle, T. D. Pilz, D. Sorsche, H. Görls and S. Rau, *Eur. J. Inorg. Chem.*, 2015, **2015**, 750–762.